In the format provided by the authors and unedited.

Slip-activated surface creep with room-temperature super-elongation in metallic nanocrystals

Li Zhong[1], Frederic Sansoz[2]*, Yang He[1], Chongmin Wang[3], Ze Zhang[4], Scott X. Mao[1]*

[1]Department of Mechanical Engineering and Materials Science, University of Pittsburgh, Pittsburgh, Pennsylvania 15261, USA.

[2]Department of Mechanical Engineering and Materials Science Program, The University of Vermont, Burlington, Vermont 05405, USA.

[3]Environmental Molecular Sciences Laboratory, Pacific Northwest National Laboratory, Richland, WA 99352, USA.

[4]Department of Materials Science and Engineering and State Key Laboratory of Silicon Materials, Zhejiang University, Hangzhou 310027, China

*Correspondence to: sxm2@pitt.edu and frederic.sansoz@uvm.edu

Supplementary Information includes:

1. Normalization of elongation

2. Strength limit in experiments estimated from MD simulations

3. Theory of nanowire thinning by slip-activated surface creep

4. Estimation of surface diffusivity

5. Supplementary Figures (S1-S18) and Tables (S1 and S2)

6. Captions for Supplementary Movies S1-S7

1. Normalization of elongation

During tensile loading of a nanowire (NW), the measured pre-necking strain can be represented by

$$\varepsilon = \frac{N\Delta L}{L},\tag{S1}$$

where N is the number of slip events before the onset of necking, ΔL is the elongation after each slip (that is, the projection of Burgers vector in the axial direction), and L is the original length of the NW. We define ω as the ratio between the neck width and the original diameter D at the onset of necking. Then

$$\Delta D N p = (1 - \omega)D\tag{S2}$$

where ΔD is the decrease in the diameter after each slip event (that is, the projection of the Burgers vector in the radial direction), and p represents the distribution of the slips, which dictates the tendency towards necking. Therefore ω is a function of p where $\omega = f(p)$. Combining Eqs. (S1) and (S2), we have A

$$\varepsilon_N = \frac{\varepsilon}{\frac{D}{L}} = \frac{1-\omega}{p}\frac{\Delta L}{\Delta D} = \frac{1-f(p)}{p}\frac{\Delta L}{\Delta D}\tag{S3}$$

Where ε_N is the normalized elongation. There are two boundaries for p:

1) When all slips occur on the same plane, then $p = 1$;

2) When slips distributed uniformly, then $\omega = \sqrt{\frac{1}{1+\varepsilon}}$, and $p = (1 - \sqrt{\frac{1}{1+\varepsilon}})\frac{D}{L}\frac{1}{\varepsilon}\frac{\Delta L}{\Delta D}$. Thus

$$\left(1 - \sqrt{\frac{1}{1+\varepsilon}}\right)\frac{D}{L}\frac{1}{\varepsilon}\frac{\Delta L}{\Delta D} \leq p \leq 1\tag{S4}$$

Since $\frac{\Delta L}{\Delta D}$ in Eq. S3 only depends on the loading orientation, the diameter dependence of ε_N mainly stems from the diameter-dependent p. In our experiments, most of specimens have aspect ratios between 0.5 and 2. From a pure dislocation plasticity perspective, the deformation mode in all our samples should be similar[1], leading to similar p and $f(p)$. As a result, without taking surface diffusion into account, ε_N should have a negligible size dependence. The slight size dependence of ε_N observed in Ag nanocrystals with diameters above 15 nm (Fig. 1h) mainly reflects the impact of surface diffusion on p through slip-activated surface creep. The normalized elongation is found to be independent of the aspect ratio (Supplementary Fig. S5), demonstrating that the geometrical factor has been

effectively minimized by this normalization method. Note that in Ag NWs with a high aspect ratio of ~35 and a five-fold twinned structure[2], deformation mode and thus both p and $f(p)$ are different than those in our study, thus making direct comparison of normalized elongation difficult.

2. Strength limit in experiments estimated from MD simulations

Kinetic theory based on surface dislocation nucleation in metallic nanowires has established that the temperature and strain-rate dependence of the nucleation stress σ_c is sensitive to activation energy and activation volume at the nanoscale[3,4]. As a first approximation, Zhu et al[3]. have proposed that

$$\sigma_c = \sigma_{ath} - \frac{k_B T}{\Omega^*} \ln\left(\frac{k_B T N \nu_D}{E \dot{\varepsilon} \Omega^*} \right) \tag{S5}$$

where σ_{ath} is the athermal nucleation stress near 0 K, Ω^* is the activation volume, T is the temperature, k_B is the Boltzmann constant, N is the number of nucleation site (here we assume $N=1$ for simplicity), ν_D is the Debye frequency, E is the Young's modulus, and $\dot{\varepsilon}$ is the strain rate.

The Debye frequency is given by

$$\nu_D = \left(\frac{3n}{4\pi V} \right)^{1/3} \nu_s \tag{S6}$$

where n/V is the atom number density used in our MD simulation, and ν_s is the sound speed.

Furthermore, Deng and Sansoz[5] found from MD simulations in different types of fcc metal nanowires that σ_{ath} is given by

$$\sigma_{ath} = \frac{4\gamma_{usf}}{b} \beta - \sigma_0 \tag{S7}$$

where γ_{usf} is the unstable stacking-fault energy of the metal, b is the Burgers vector of the partial Shockley dislocation, β is a geometrical factor accounting for the Schmid factor and shape factor, and σ_0 is an image stress resulting from the contribution of free surfaces,

which can be considered to scale as $1/D$ (Supplementary Ref. 6). For convenience, we re-write Eq. (S7) as

$$\sigma_{ath} = \sigma^{max} - \frac{\Gamma}{D} \tag{S8}$$

where σ^{max} is the ideal nucleation stress and Γ is an image stress factor. Here, Ω^*, σ^{max}, and Γ were used as fitting parameters to match the strength model to MD simulation results. The parameters σ^{max} and Γ in Equation (S8) were first determined by fitting the results of MD simulations in double-conical <112> nanowires with different diameters at the narrowest section between 5 nm and 30 nm (the wider diameter was kept 4 nm larger than the smaller diameter in all cases) deformed at a temperature of 0.1K (Supplementary Fig. S8a). The activation volume Ω^* in Eq. (S5) was identified by performing MD simulations at 300K in a nanowire with different diameters (Supplementary Fig. S8a). A cross-check to assess the goodness of fit was also carried out by performing additional simulations at different strain rates at 300 K in a nanowire of 20 nm in diameter (Supplementary Fig. S8b). The strength parameters for the Ag model are shown in Supplementary Table S1. Supplementary Fig. S8b shows good agreement between our theoretical predictions from this model and the experimental in-situ TEM measurements in Ag nanocrystals deformed at 300K and strain rates on the order of 10^{-3} s^{-1} (Supplementary Fig. S7).

3. Theory of nanowire thinning by slip-activated surface creep

3.1. Rate of thinning by crystal slip

The rate of nanowire thinning from crystal slip by surface dislocation emission can be obtained by

$$\frac{\Delta D}{\Delta t} = \frac{\Delta s}{\Delta t} \sin\alpha \tag{S9}$$

where s is the total slip length and α is the projected angle with respect to the <112> loading direction of the {111}<110> slip, as schematically shown in Supplementary Fig. S16a. During the slip event, the nanowire continues to deform plastically as long as the tensile

stress in the slipped region is equal to or larger than the tensile yield stress required to emit new partial dislocations, σ_c, which leads to an equilibrium slip length given by[1]

$$s = \frac{E\varepsilon - \sigma_c}{E\cos\alpha - \left(\dfrac{L}{D}\right)\sigma_c \sin\alpha} L \tag{S10}$$

where E is the Young's modulus in the <112> direction, and L and D are the initial length and diameter of the nanowire before slip, respectively. Therefore, the thinning rate can be expressed as a function of applied strain rate such as

$$\frac{\Delta D}{\Delta t} = \frac{L\sin\alpha}{\cos\alpha - \left(\varepsilon_0 \dfrac{L}{D}\right)\sin\alpha} \dot{\varepsilon} \tag{S11}$$

where ε_0 is the elastic strain limit taken as $\varepsilon_0 = \sigma_c/E$.

3.2. Rate of thinning by surface atom diffusion

Torres *et al.*[7] analyzed the thinning of a stress-free tip-suspended cylindrical nanowire based on surface diffusion, in terms of a thermodynamic tip suction driving migration of surface from the wire to the tip, as shown in Supplementary Fig. S16b. We have extended this concept to take into account the driving force emanating from the applied strain and the shape change of the nanowire ends. We find that the potential drop of a surface atom from the middle to one end of the nanowire can be presented as

$$\Delta E \approx -\left(\frac{2\gamma}{D\rho} + \frac{15E\varepsilon_0^2}{32\rho}\right) \tag{S12}$$

where D is here taken as the diameter in the middle of the nanowire (that is, the smallest diameter of the nanowire), γ is the surface energy and ρ is the bulk density. The values of E and γ for different metals are derived from those presented in Supplementary Refs. 8 and 9, respectively. The following assumptions were made. First, we consider a nanowire with gradient in radius, e.g., R_1 in the middle and R_2 at both ends as shown in Supplementary Fig. S16c. Thus

$$\Delta E_1 = \frac{\gamma}{\rho}\left(\frac{1}{R_2} - \frac{1}{R_1}\right) \tag{S13}$$

Second, the difference in the elastic energy of surface atoms in the middle and at the end of the nanowires was considered to be

$$\Delta E_2 = \frac{E}{2\rho}(\varepsilon_2^2 - \varepsilon_1^2) \tag{S14}$$

where ε_1 and ε_2 are the lattice strains at the middle and end of the nanowire, respectively, such as $\varepsilon_2 = \frac{R_1^2}{R_2^2}\varepsilon_1$. Since the middle of the nanowire has the smallest diameter, ε_1 equals to the elastic limit ε_0 (that is, the lattice strain for dislocation nucleation). This gives

$$\Delta E_2 = \frac{E\varepsilon_0^2}{2\rho}\left(\frac{R_1^4}{R_2^4} - 1\right) \tag{S15}$$

Third, as shown in Supplementary Fig. S16c, a series of surface steps form a stable curved contour (with radius of R_3) that connects the NW to the substrate. Such a negative curvature contributes to a drop of ΔE_3 in the chemical potential of surface sites at the end of the NW, where ΔE_3 is given by

$$\Delta E_3 = -\frac{\gamma}{R_3\rho} \tag{S16}$$

In summary, the total energy change for a surface atom migrating from the middle to either end of the nanowire is

$$\Delta E = \Delta E_1 + \Delta E_2 + \Delta E_3 = \frac{\gamma}{\rho}\left(\frac{1}{R_2} - \frac{1}{R_1} - \frac{1}{R_3}\right) + \frac{E\varepsilon_0^2}{2\rho}\left(\frac{R_1^4}{R_2^4} - 1\right) \tag{S17}$$

Based on our experimental observations, we use $R_1/R_2 = 0.5$ and $R_2 \sim R_3$ with $R_1/D = 0.5$, which reduces Eq. (S17) into Eq. (S12). For simplicity, we also assume the potential drop (ΔE) distributes uniformly along the x axis from $x = 0$ to $x = L/2$ (Supplementary Fig. S16c). Then, the average velocity of surface atoms drifting from the wire middle towards the bulk tip, is

$$v = -\mu_s\left(\frac{2\Delta E}{L}\right) \qquad (S18)$$

where μ_s is the surface mobility given by

$$\mu_s = \frac{D_s}{k_B T} \qquad (S19)$$

with D_s being the surface diffusion coefficient. Since the average drifting distance is approximately $\Delta x = L/4$, it results that the average time of atom drifting is

$$\Delta t \approx \frac{L}{4v} = -\frac{L^2}{8\mu_s \Delta E} \qquad (S20)$$

Therefore, the rate of nanowire thinning by surface diffusion is given by

$$\frac{\Delta D}{\Delta t} = \frac{\delta_s}{\Delta t} = -\frac{8\delta_s \mu_s \Delta E}{L^2} = \frac{8\delta_s \mu_s}{L^2 \rho}\left[\frac{2\gamma}{D} + \frac{15 E \varepsilon_0^2}{32}\right] \qquad (S21)$$

where $\delta_s = 2r_0$ is the thickness of drifting surface atoms and $\rho = \frac{3}{4\pi r_0^3}$ with r_0 the atomic radius. All model parameters for Ag and Pt nanocrystals are shown in Supplementary Table S2.

4. Estimation of surface diffusivity

The surface diffusivity of nanocrystals was estimated from the shape evolution of free-standing nano-tips. Although the nano-tips maintained a well-defined fcc structure during retraction, the surface of the sharp tip formed right after fracture was not well faceted (Supplementary Fig. S18 and Movie S7), indicating the validity of estimating the diffusivity by curvature-driven surface diffusion theory without considering the slow kinetics controlled by facet nucleation[10]. As a result, the surface diffusivity D_s can be approximately represented as[11]

$$D_s \approx \frac{R^3 h k_B T}{\tau \gamma \Omega \delta_s} \qquad (S22)$$

where R is the radius of curvature at the sharp tip end, h is the reduction in the tip height (that is, the retraction distance), k_B is the Boltzmann constant, γ is the surface energy, and Ω is the atomic volume. T is the absolute temperature, which is ~300 K in the current study, and δ_s is the surface layer thickness with a value of ~0.25 nm (that is, one atomic layer thickness). R and h were directly measured from the shape evolution of the tip during a time period of τ.

For Ag nano-tips, R = 4 nm, h = 0.4 nm, τ = 0.5 s, $\Omega \sim 1.25 \times 10^{-29}$ m^{-3}, and γ = 1.17 J·m^{-2}, which leads to $D_s = 5.8 \times 10^{-17}$ m^2·s^{-1}.

In the case of Pt nano-tips, R = 0.3 nm, h = 0.3 nm, τ = 0.3 s, $\Omega \sim 1.1 \times 10^{-29}$ m^{-3}, and γ = 2.3 J·m^{-2}, resulting in $D_s = 1.8 \times 10^{-20}$ m^2·s^{-1}.

5. Supplementary Figures and Tables
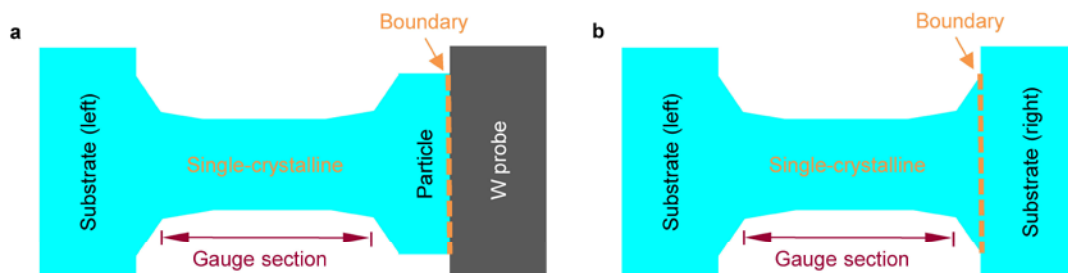
Figure S1. Schematics showing the geometry of single-crystalline gauge sections. a, Specimens prepared via welding together one nano-tip and one particle deposited on a W probe. **b,** Specimens formed by welding together two nano-tips.
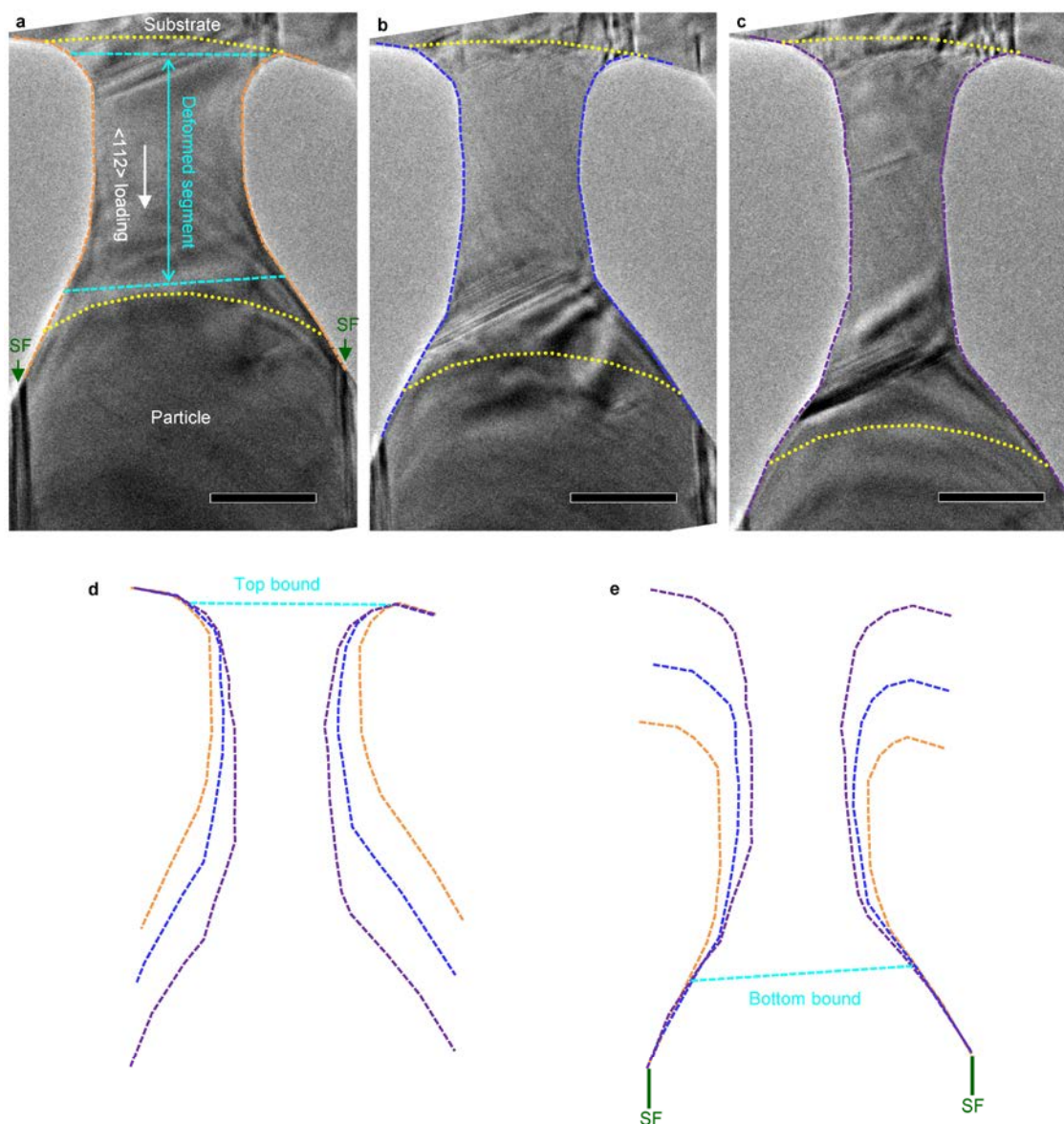
Figure S2. Plastic deformation within the gauge section. a-c, Sequential images of a 28-nm-diameter single-crystalline Ag segment under tensile loading (extracted from Supplementary Movie S1). Two vertical stacking faults (SFs) indicated by green arrow heads are used as two reference points. All scale bars are 20 nm. **d,e,** Determination of the deformed segment by tracking the shape evolution of the nanocrystal. The top (**d**) and bottom (**e**) bounds of the deformed region (cyan dash lines) are plotted in **a**, clearing demonstrating that plastic deformation proceeds within the gauge section (outlined by yellow dotted lines).
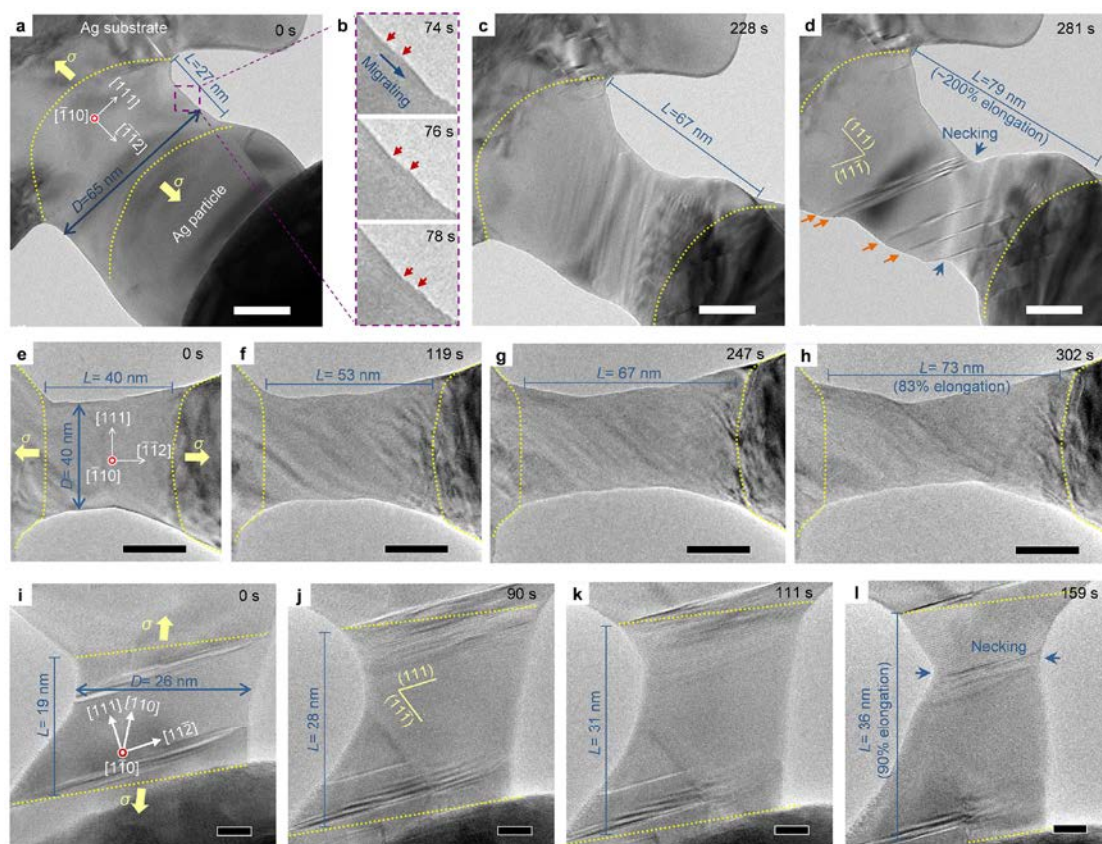
Figure S3. Superplastic behavior of Ag nanocrystals with diameters in the range of 15-80 nm along different loading directions. a-d, A short Ag junction with a diameter of 65 nm exhibited ~200% elongation before the onset of necking under <112> tensile loading at a strain rate of 9×10^{-3} s^{-1}. Both surface step migration (indicated by red arrows in **b**) and crystal slips (marked by orange arrows in **d**) were captured during deformation. **e-h,** Tensile straining of a 40-nm-diameter Ag nanocrystal along the <112> direction led to a uniform elongation of 83% under a strain rate of 3×10^{-3} s^{-1}. **i-l,** Uniform elongation of a 26-nm-diameter Ag nanocrystal up to ~90% along the <110> direction at a strain rate of 7×10^{-3} s^{-1}. The gauge sections are outlined by yellow dotted curves. Scale bars are 20 nm (**a, c-h**) and 5 nm (**i-l**).
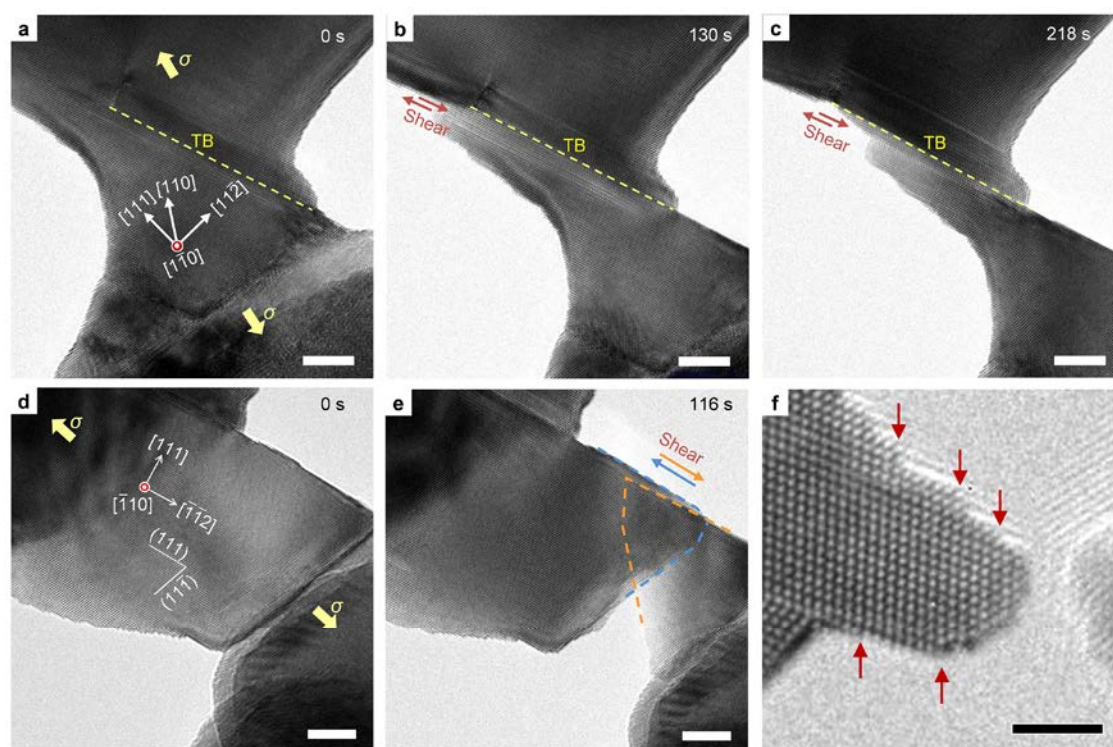
Figure S4. Plastic instability and absence of surface diffusion in Pt nanocrystals. a-c, Sequential images showing rigid-shear-like deformation at the vicinity of a twin boundary (TB) in a 22-nm-diameter Pt nanocrystal. **d,e,** localized shear on inclined slip planes by either $[\bar{1}01](1\bar{1}1)$ or $[0\bar{1}1](\bar{1}11)$ dislocation slips during tensile straining of a 25-nm-diameter Pt nanocrystal along the $[\bar{1}\bar{1}2]$ direction. **f,** Lack of surface diffusion on a sharp Pt tip. Immobile surface steps are indicated by red arrows. Scale bars are 5 nm (**a-e**), and 2 nm (**f**).
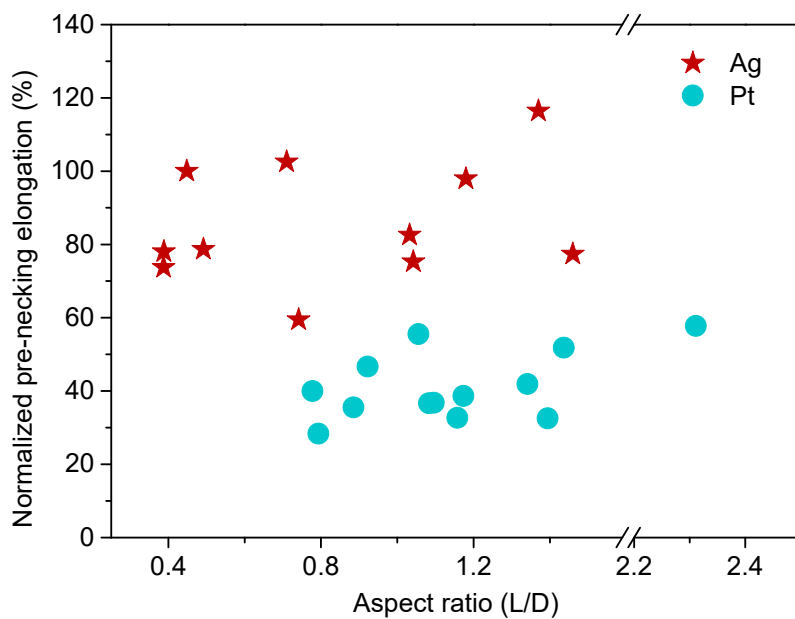
Figure S5. Normalized pre-necking elongation as a function of aspect ratio. To minimize size and strain rate effects, Ag samples with diameters below 15 nm were excluded, and the applied strain rates were on the order of 10^{-3} s^{-1}.
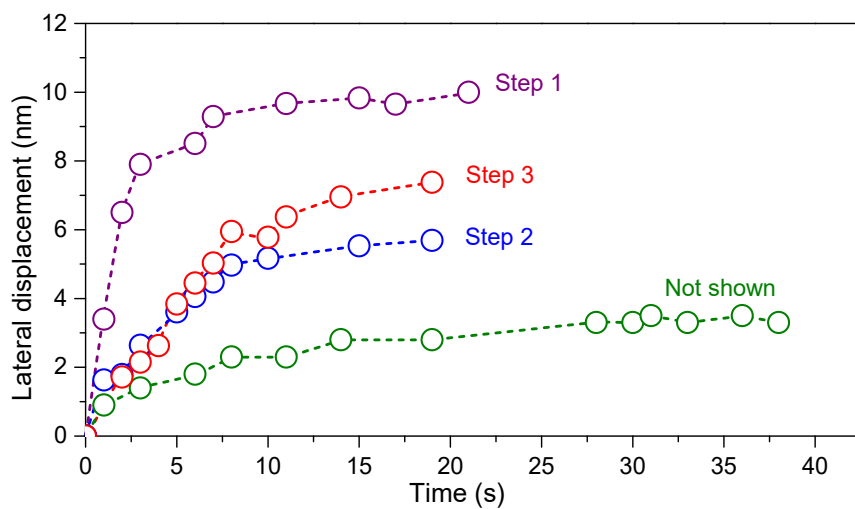
Figure S6. Lateral displacement as a function of time measured from four surface steps. Steps 1-3 correspond to step motions tracked by purple, blue, and red arrows in Fig. 2, respectively. The green curve was measured from a surface step nucleated before Step 1.
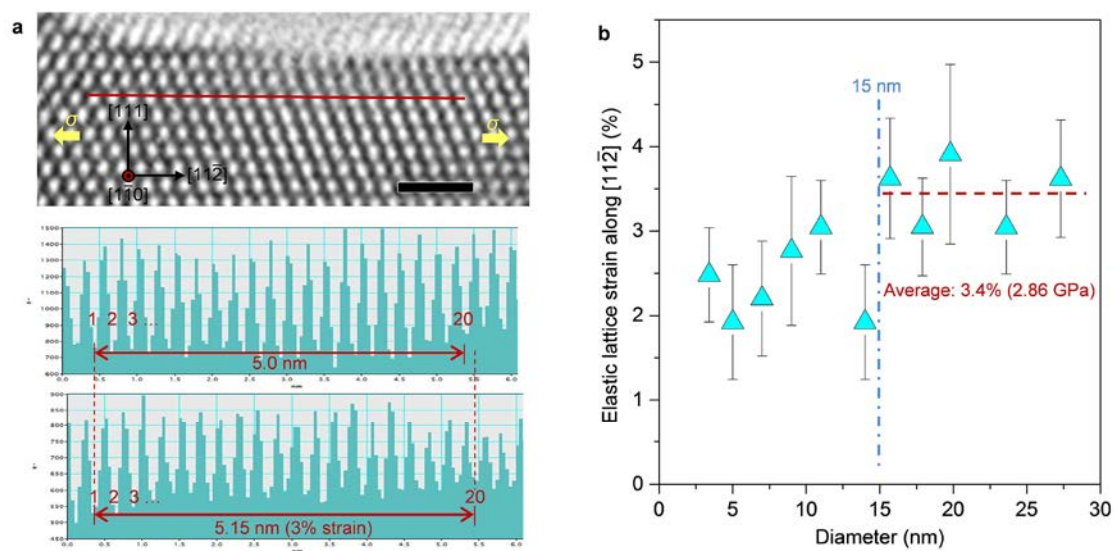
Figure S7. Elastic strain of Ag nanocrystals under <112> tensile deformation at strain rates on the order of 10^{-3} s^{-1}. a, Elastic strain was obtained by measuring the lattice expansion along the loading direction. For example, an elastic strain of 3% was measured in the $[11\bar{2}]$ direction. The scale bar is 1 nm. **b,** The average elastic strain reached ~3.4% in Ag nanocrystal with diameters above 15 nm, corresponding to a stress of ~2.86 GPa. It, however, reduced quickly when the nanocrystal diameter dropped below the diffusion stability limit around 15 nm due to softening caused by dominant surface creep. Error bars represent the variation in the lattice strains measured at different locations of a nanocrystal.
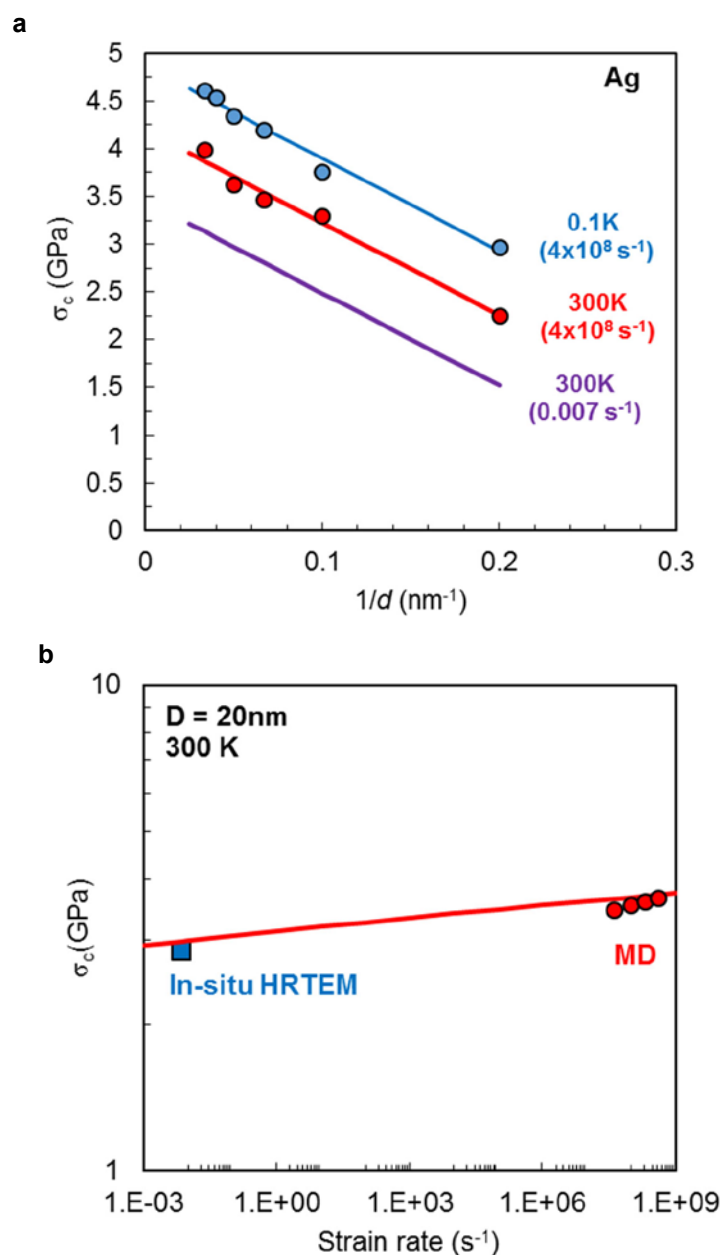
Figure S8. Simulated tensile yield stress in Ag nanowires for fitting of strength model parameters. a, Effect of diameter at 0.1 K and 300 K. **b,** Strain-rate effect in a 20-nm-diameter Ag nanowire at 300 K. Limit of elasticity measured experimentally by in-situ high-resolution TEM is shown with a square symbol. Solid lines represent theoretical predictions from strain-rate dependent dislocation nucleation model at different temperatures and strain rates.
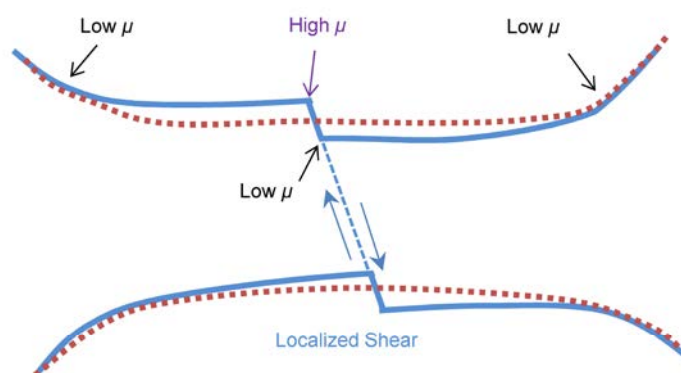
Figure S9. Schematics depicting the role of surface diffusion in suppressing plastic instability resulting from crystal slips. Slip-induced shear localization leads to an abrupt change in the surface contour (blue solid contour) associated with local differences in chemical potential μ. Surface diffusion mediated by the high stress and curvature change stimulates atom migration from sites with large positive curvatures (high μ) to those with negative curvatures (low μ), thereby improving plastic stability by maintaining a smooth and uniform surface contour (red dash-line contour).
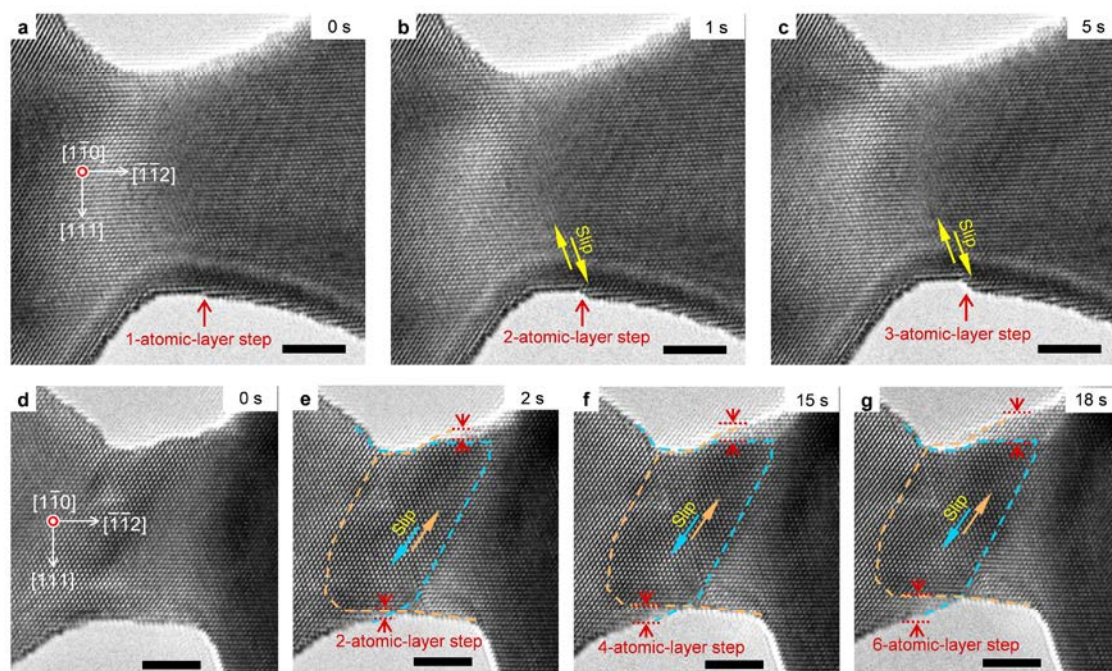
Figure S10. Localized consecutive crystal slips at surface steps in Pt nanocrystals. a-c, Localized crystal slips along either the [101] or [011] direction on the (11$\bar{1}$) slip plane. **d-g,** Localized crystal slips along the [110] direction on either the ($\bar{1}$11) or (1$\bar{1}$1) inclined slip plane. All scale bars are 3 nm.
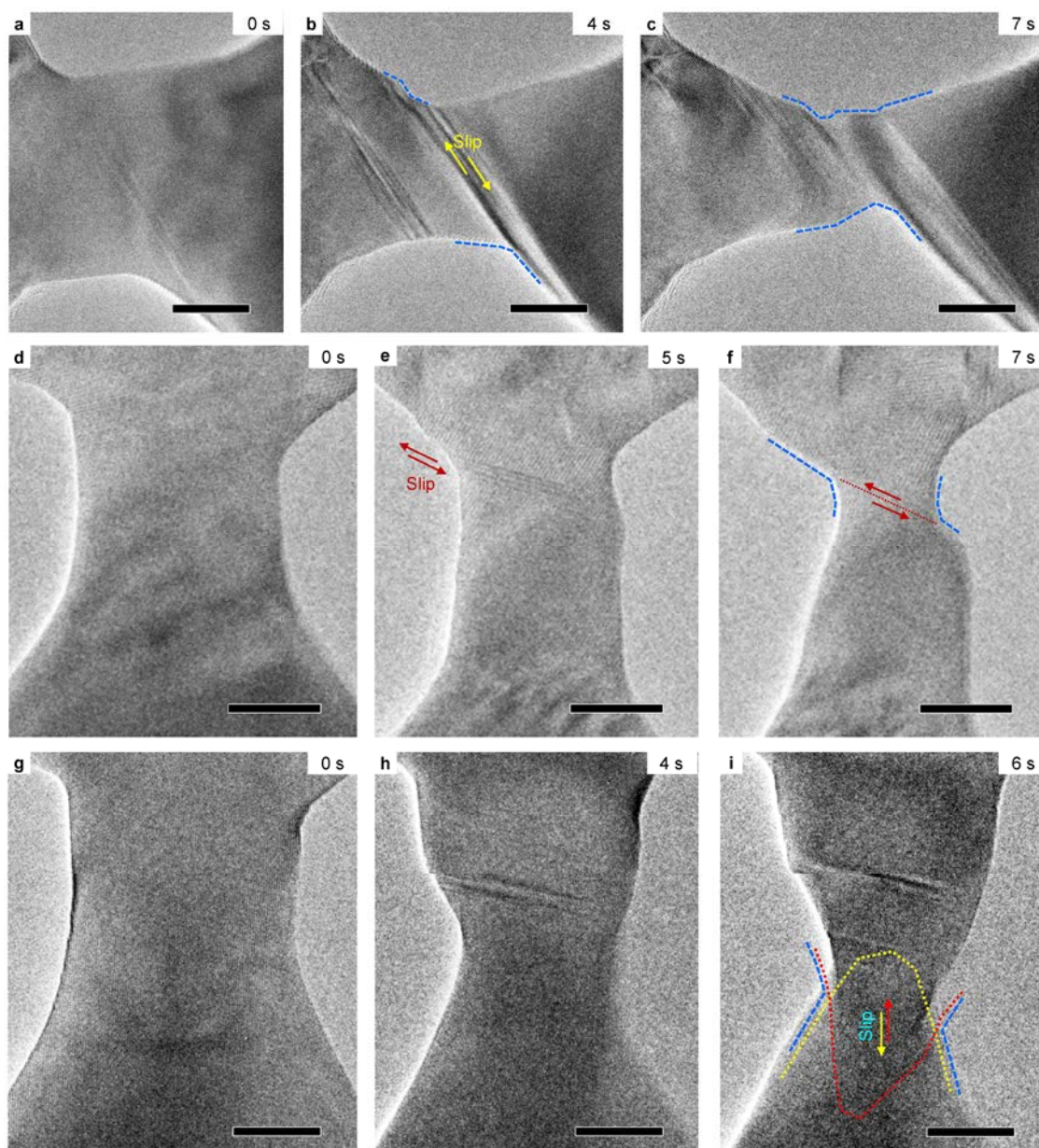
Figure S11. Localized crystal slips and limited ductility of Ag nanocrystals under high strain rates of, a-c, 0.1 s^{-1}, d-f, 0.07 s^{-1}, and, g-i, 0.08 s^{-1}. The arrows indicate the slip directions and the blue dash lines outline the abrupt changes in the contour of the nanocrystal due to localized crystal slips. All scale bars are 10 nm.
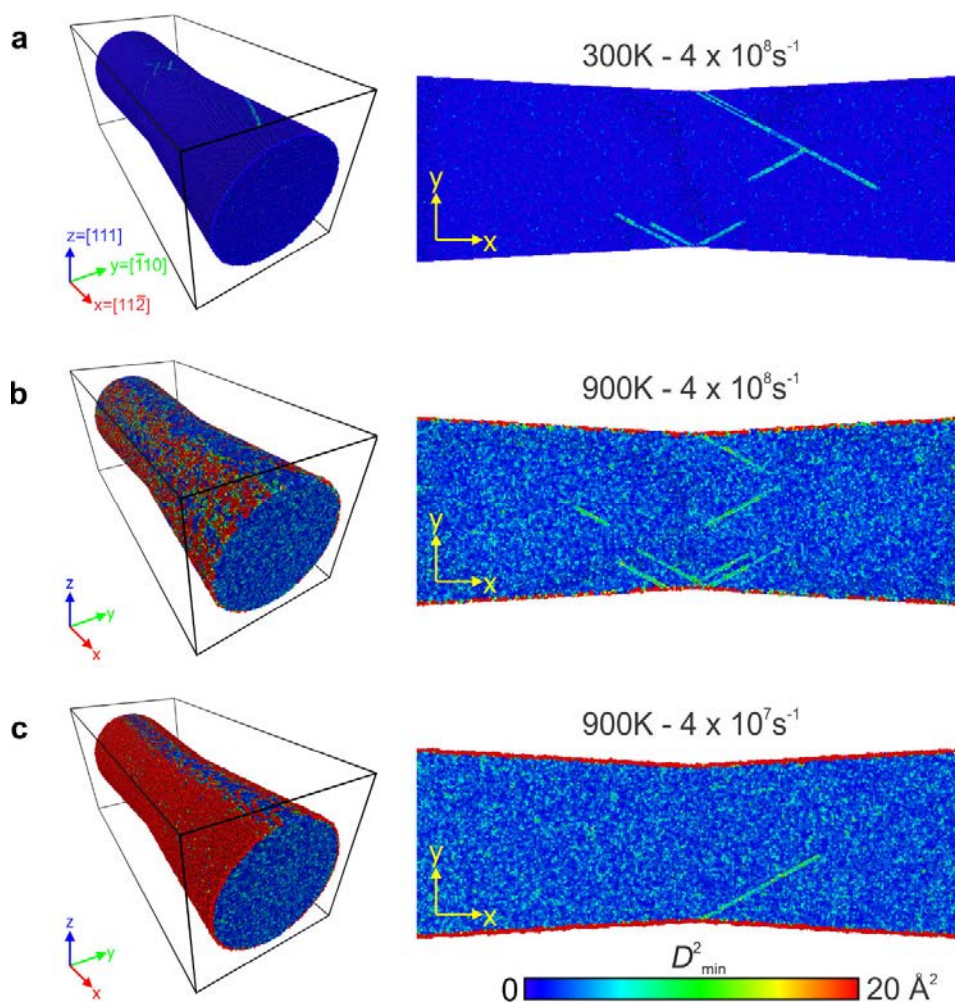
Figure S12. Non-affine squared displacement (D^2_{min}) at the onset of surface dislocation nucleation in a <112>-oriented single-crystal Ag nanowire deformed at, **a,** temperature of 300 K and strain rate of 4×10^8 s^{-1}, **b,** temperature of 900 K and strain rate of 4×10^8 s^{-1}, **c,** temperature of 900 K and strain rate of 4×10^7 s^{-1}.
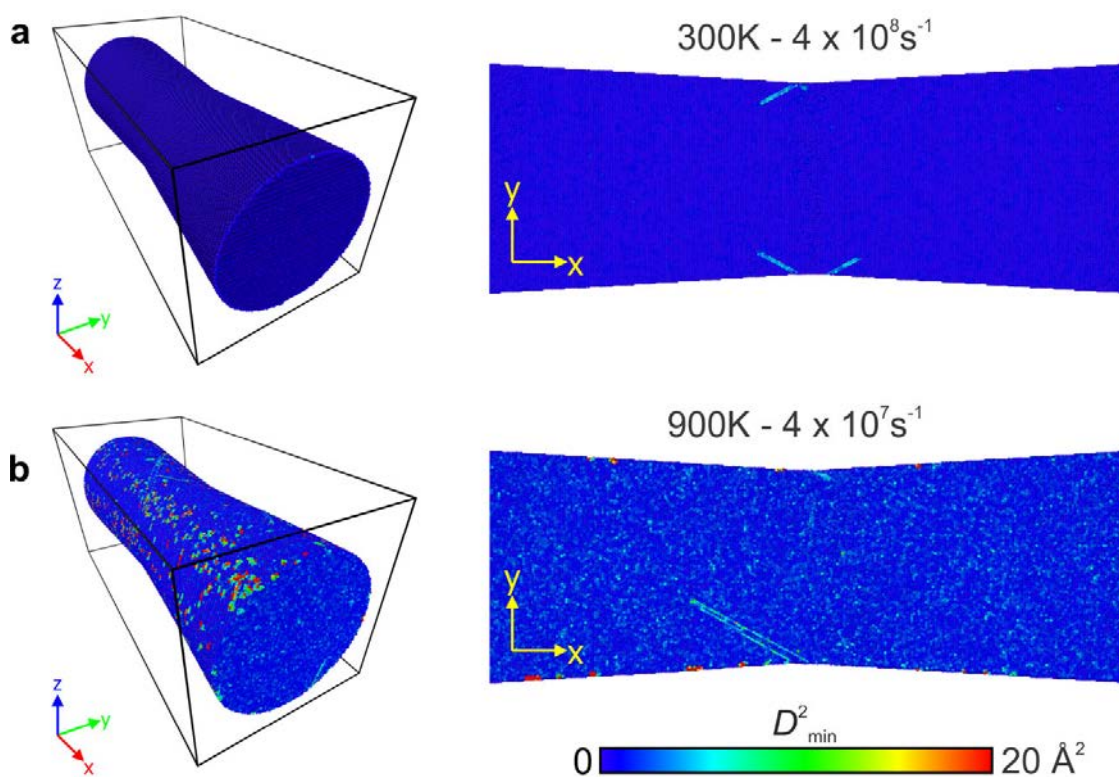
Figure S13. Non-affine squared displacement (D^2_{min}) at the onset of surface dislocation nucleation in a <112>-oriented single-crystal Pt nanowire deformed at, **a,** temperature of 300 K and strain rate of 4×10^8 s^{-1}, and, **b,** temperature of 900 K and strain rate of 4×10^7 s^{-1}.

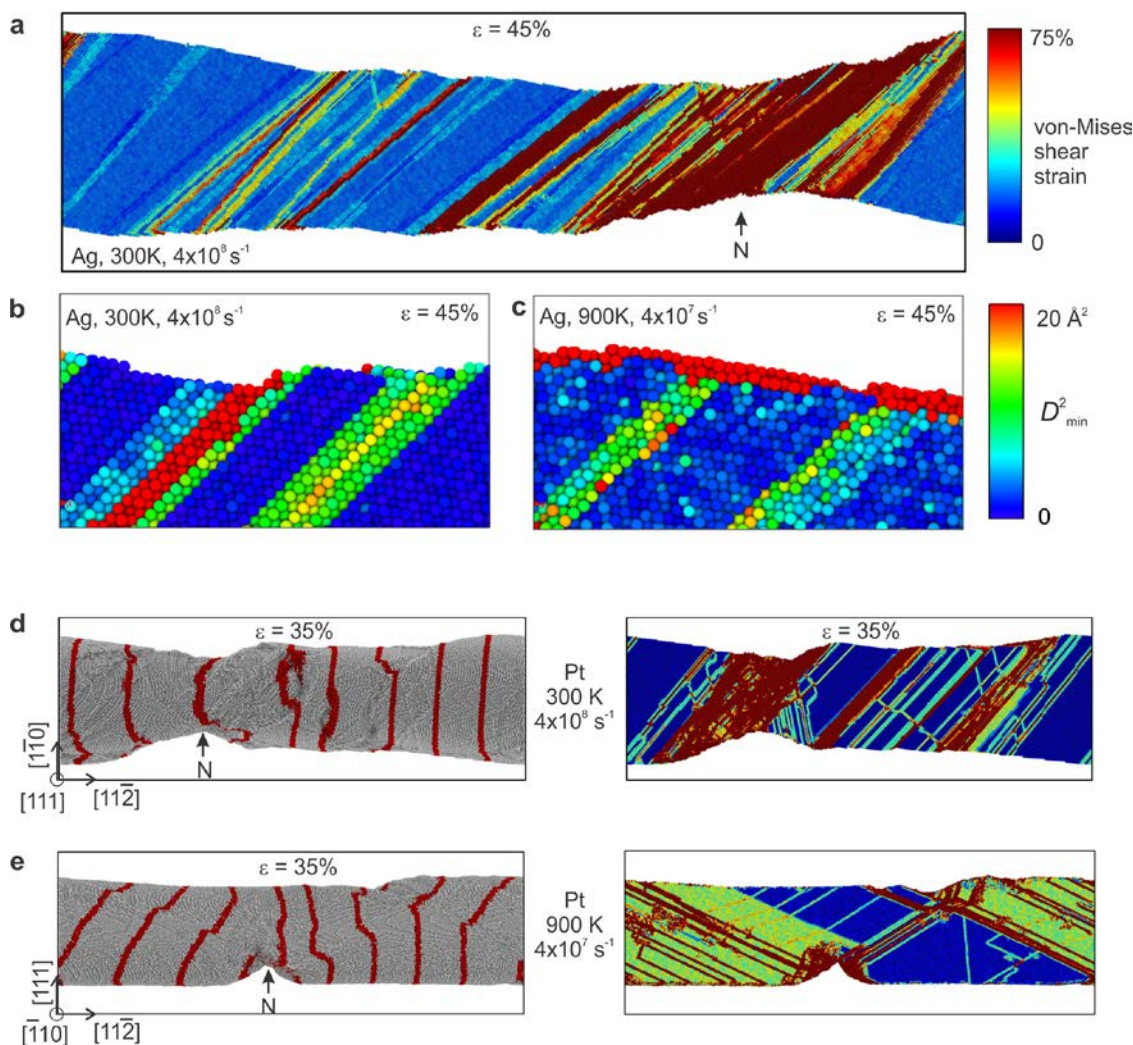**Figure S14. MD simulations of plasticity and necking at large strains in <112>-oriented double-conical-shaped Ag and Pt NWs. a,** Atomic shear strain in Ag NW deformed by 45% strain at 300 K and a strain rate of 4×10^8 s^{-1}. **b,c,** Non-affine squared displacement (D_{min}^2) at the surface of two Ag NWs deformed by 45% strain at 300 K and a strain rate of 4×10^8 s^{-1} (**b**), and at 900 K and a strain rate of 4×10^7 s^{-1} (**c**). **d,e,** Snapshots of plastic deformation and local shear strain in Pt NWs deformed by 35% strain at 300 K and a strain rate of 4×10^8 s^{-1} (**d**), and 900 K and a strain rate of 4×10^7 s^{-1} (**e**). In **d** and **e**, red vertical markers have been added to highlight the initial position of atoms present on several surface steps.
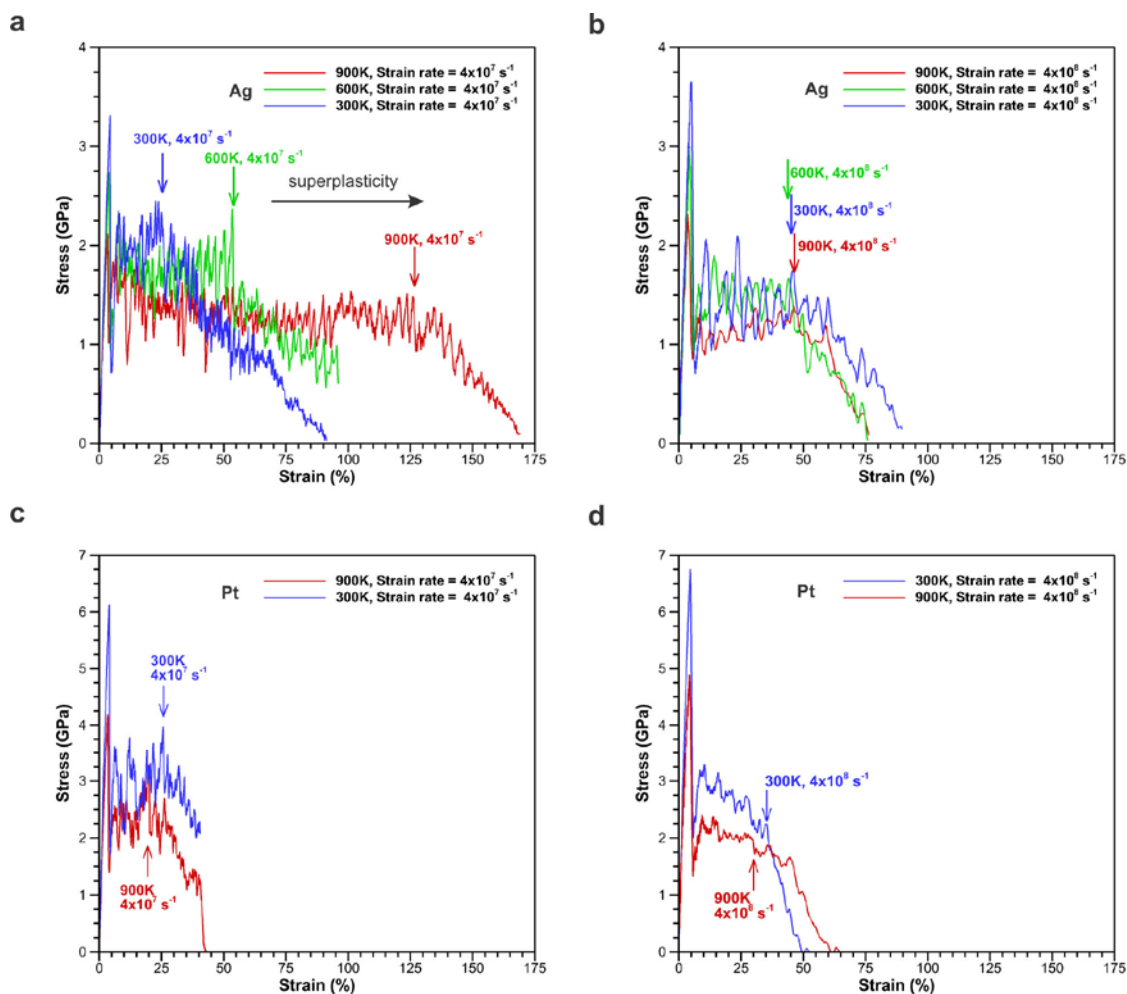
Figure S15. Stress-strain curves obtained by MD simulations of tensile straining of <112>-oriented double-conical-shaped Ag and Pt NWs at different temperatures. a,b, Stress-strain curves of Ag NWs at strain rates of 4×10^7 s^{-1} (**a**) and 4×10^8 s^{-1} (**b**). **c,d,** Stress-strain curves of Pt NWs at strain rates of 4×10^7 s^{-1} (**c**) and 4×10^8 s^{-1} (**d**). Vertical arrows above the curves show the onset of necking during plastic deformation of the nanowire as observed from simulation snapshots.
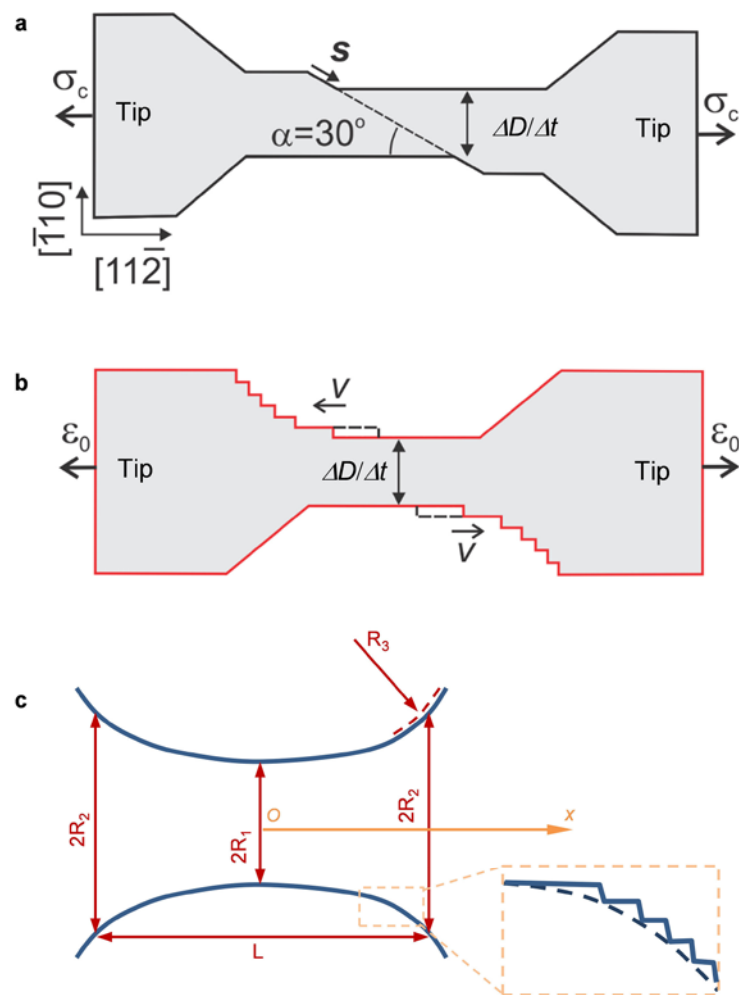
Figure S16. Schematics of nanowire thinning by crystal slip and surface diffusional creep. a, Thinning by crystal slip. **b,** Thinning by surface step diffusion. **c,** Side contour of a nanowire with diameter gradient. The inset is a close-up view of the surface curvature composed of surface steps.
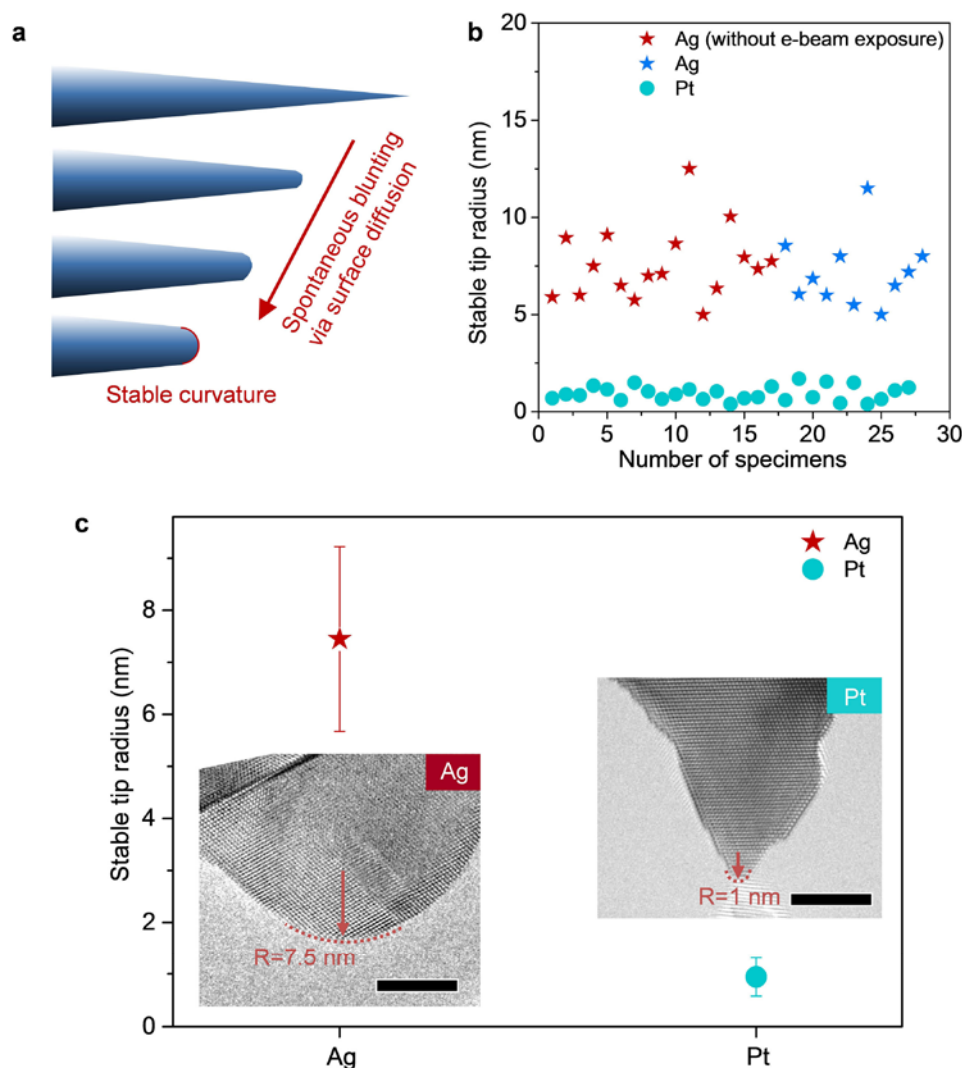
Figure S17. Diffusion stability limit for slip-activated surface creep. a, Schematic illustration of the surface-diffusion-mediated shape evolution of a tapered NW. The gradual increase in the radius of curvature at the NW tip results in a diminishing driving force for surface diffusion, leading to stabilization of the curvature when the driving force is no longer significant enough to overcome the energy barrier for surface diffusion. **b,** Stable tip radii of Ag and Pt NWs. Red stars represent the stable radii of Ag tips that were kept away from the electron beam during shape evolution, except for an exposure time of ~1 s for image recording. Note that minimal impact of electron-beam irradiation on the tip radius of Ag was observed. **c,** Statistical study on the stable tip radii of Ag and Pt NWs. Error bars represent the variation among the stable tip radii of multiple specimens. The insets are high-resolution TEM images of the self-blunted tips. Scale bars are 5 nm.

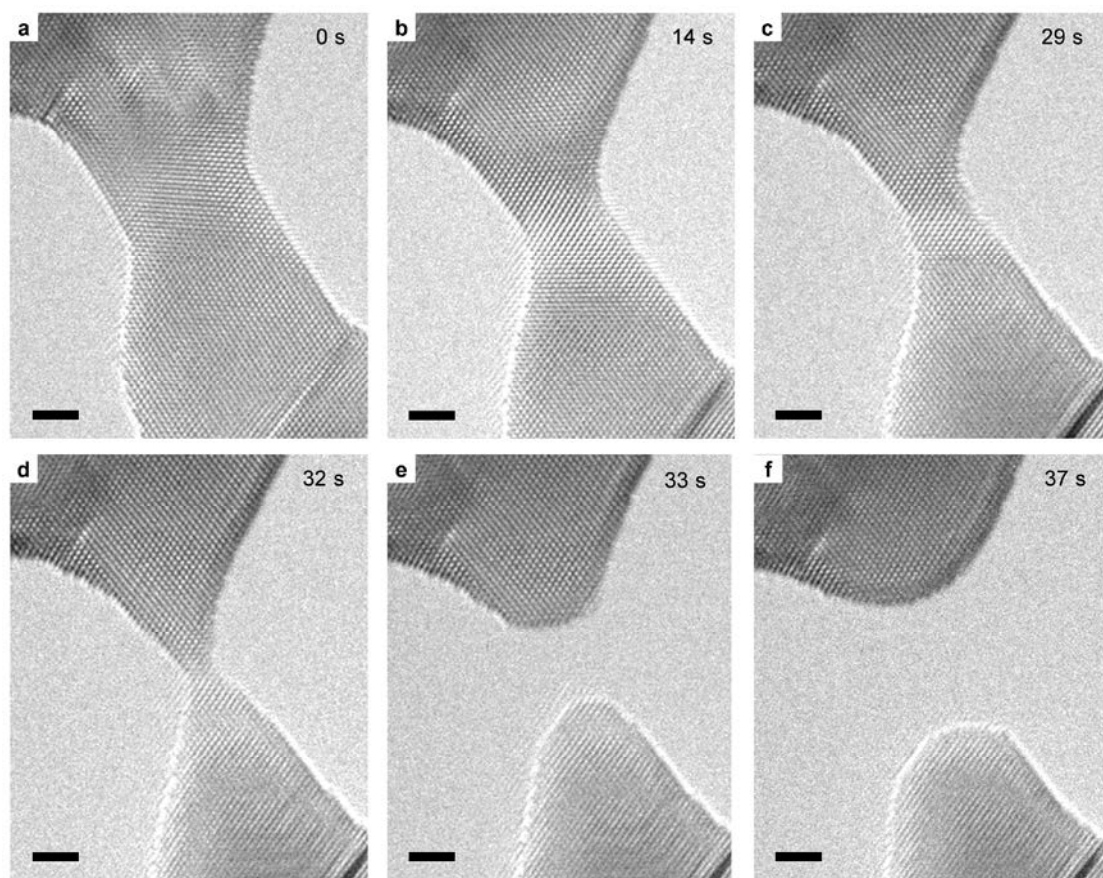**Figure S18. Liquid-like behavior in a Ag nanocrystal with size below the diffusion stability limit. a-d,** Rapid necking during tensile loading. **e,f,** Surface-diffusion-mediated spontaneous tip-blunting after fracture. All scale bars are 2 nm.

Table S1. Model parameters used in strength limit estimate.

	Ag Nanowire
Young's modulus E (GPa)	84.1
Temperature T (K)	300
Ideal nucleation stress σ^{max} (GPa)	4.87
Image stress factor Γ (Pa·m)	9.7
Total volume V (Å^3)	25,516,727
Number density (m^{-3})	5.82E+28
Sound speed (m·s^{-1})	3.65E+3
Debye frequency (Hz)	8.77E+12
k_B (J/K)	1.38E-23
Burgers vector b (nm)	0.167
Activation volume Ω^* (b^3)	30

Table S2. Model parameters used in thinning rate theory based on crystal slip and surface diffusion.

	Ag	Pt
Temperature (K)	300	300
Young's modulus E (GPa)	84.1	185.3
Projected slip angle α (deg.)	30	30
Elastic strain limit	0.03	0.03
Engineering strain rate (s^{-1})	7.00E-03	8.00E-03
Surface energy γ (J/m^2)	1.17	2.3
Atomic radius r_0 (nm)	0.165	0.177
Surface diffusivity D_s (m$^2 \cdot$s^{-1})	5.8E-17	1.8E-20
Surface mobility μ_s (m$^2 \cdot$J$^{-1} \cdot$s^{-1})	1.4E+4	4.3

6. Captions for Supplementary Movies S1-S7

Movie S1. Super-elongation of a <112>-oriented 28-nm-diameter Ag nanocrystal at a strain rate of ~3×10^{-3} s^{-1}. The movie is played at a speed of 10×.

Movie S2. Super-elongation and gradual ductile necking of a <112>-oriented 65-nm-diameter Ag nanocrystal at a strain rate of ~9×10^{-3} s^{-1}. The movie is played at a speed of 15×.

Movie S3. Premature necking due to localized shear during <112> tensile straining of a 14-nm-diameter Pt nanocrystal at a strain rate of ~2×10^{-3} s^{-1}. The movie is played at a speed of 15×.

Movie S4. Surface ledge flow mediated by slip-activated surface diffusion during <112> tensile straining of a 20-nm-diameter Ag nanocrystal. The movie is played at a speed of 2×.

Movie S5. Molecular dynamics simulation of tensile straining of a Ag nanowire at 900 K and a strain rate of 4×10^{7} s^{-1} showing superplasticity behavior up to 126% strain accompanied by prominent surface atom diffusion. The time interval between each frame is 62.5 ps. Red vertical markers have been added to highlight the initial position of atoms on selected surface steps.

Movie S6. Molecular dynamics simulation of tensile straining of a Ag nanowire at 900 K and a strain rate of 4×10^{8} s^{-1} showing early necking and plastic instability at 45% strain with negligible surface atom diffusion. The time interval between each frame is 12.5 ps. Red vertical markers have been added to highlight the initial position of atoms on selected surface steps.

Movie S7. Shape evolution of a free-standing sharp Ag nano-tip via curvature-driven surface diffusion. The movie is played at a speed of 6×.

Supplementary References

1   Wu, Z. X., Zhang, Y. W., Jhon, M. H., Gao, H. J. & Srolovitz, D. J. Nanowire failure: long = brittle and short = ductile. *Nano Lett.* **12**, 910-914 (2012).

2   Filleter, T. *et al.* Nucleation-controlled distributed plasticity in penta-twinned silver nanowires. *Small* **8**, 2986-2993 (2012).

3   Zhu, T., Li, J., Samanta, A., Leach, A. & Gall, K. Temperature and strain-rate dependence of surface dislocation nucleation. *Phys. Rev. Lett.* **100**, 025502 (2008).

4   Zhu, T. & Li, J. Ultra-strength materials. *Prog. Mater Sci.* **55**, 710-757 (2010).

5   Deng, C. & Sansoz, F. Fundamental differences in the plasticity of periodically twinned nanowires in Au, Ag, Al, Cu, Pb and Ni. *Acta Mater.* **57**, 6090-6101 (2009).

6   Hirth, J. P. & Lothe, J. *Theory of dislocations*. 2 edn,   (Wiley, 1982).

7   Torres, J. A. *et al.* The puzzling stability of monatomic gold wires. *Surf. Sci.* **426**, L441-L446 (1999).

8   Cagin, T., Dereli, G., Uludogan, M. & Tomak, M. Thermal and mechanical properties of some fcc transition metals. *Phys. Rev. B* **59**, 3468-3473 (1999).

9   Vitos, L., Ruban, A. V., Skriver, H. L. & Kollar, J. The surface energy of metals. *Surf. Sci.* **411**, 186-202 (1998).

10 Combe, N., Jensen, P. & Pimpinelli, A. Changing shapes in the nanoworld. *Phys. Rev. Lett.* **85**, 110-113 (2000).

11 Tian, L., Li, J., Sun, J., Ma, E. & Shan, Z. W. Visualizing size-dependent deformation mechanism transition in Sn. *Sci. Rep.* **3**, 2113 (2013).